Geological Society of America Bulletin
June 2023, Volume 136 Issue 3/4 Pages 917-627
https://doi.org/10.1130/B36859.1
https://archimer.ifremer.fr/doc/00883/99492/

Intermediate water warming caused methane hydrate instability in South China Sea during past interglacials

Li Niu [1, 2], Wang Xudong [3], Feng Junxi [4], Chen Fang [4], Zhou Yang [4], Wang Maoyu [5], Chen Tianyu [5], Bayon Germain [6], Peckmann Jörn [7], Cheng Hai [8, 9, 10], Edwards R. Lawrence [11], Chen Duofu [2, 3], Feng Dong [2, 3, *]

[1] Key Laboratory of Ocean and Marginal Sea Geology, South China Sea Institute of Oceanology, Innovation Academy of South China Sea Ecology and Environmental Engineering, Chinese Academy of Sciences, Guangzhou 510301, China
[2] Laboratory for Marine Mineral Resources, Qingdao National Laboratory for Marine Science and Technology, Qingdao 266061, China
[3] Shanghai Engineering Research Center of Hadal Science and Technology, College of Marine Sciences, Shanghai Ocean University, Shanghai 201306, China
[4] Ministry of Land and Resources, Key Laboratory of Marine Mineral Resources, Guangzhou Marine Geological Survey, Guangzhou 510075, China
[5] State Key Laboratory for Mineral Deposits Research, School of Earth Sciences and Engineering, Nanjing University, Nanjing 210023, China
[6] IFREMER, Marine Geosciences Unit, F-29280 Plouzané, France
[7] Institute for Geology, Center for Earth System Research and Sustainability, Universität Hamburg, 20146 Hamburg, Germany
[8] Institute of Global Environmental Change, Xi'an Jiaotong University, Xi'an 710054, China
[9] State Key Laboratory of Loess and Quaternary Geology, Institute of Earth Environment, Chinese Academy of Sciences, Xi'an 710061, China
[10] Key Laboratory of Karst Dynamics, Ministry of Land and Resources, Institute of Karst Geology, Chinese Academy of Geological Sciences, Guilin 541004, China
[11] Department of Earth Sciences, University of Minnesota, Minneapolis, Minnesota 55455, USA

* Corresponding author : Niu Li, email address : dfeng@shou.edu.cn

Abstract :

Methane hydrates are widely distributed along continental margins, representing a potential source of methane to the ocean and atmosphere, possibly influencing Earth's climate. Yet, little is known about the response of methane hydrates to global climate change, especially at the timescale of glacial-interglacial cycles. Here we present a chronology of methane seepage from seep carbonates derived from a series of tens to hundreds of meters long hydrate-bearing sediment records from the South China Sea, drilled at water depths of 664−871 m. We find that six out of seven episodes of intense methane seepage during the last 440,000 years were related to hydrate dissociation, all coinciding with major interglacials, the so-called Marine Isotope Stages 1, 5e, 7c, 9c, and 11c. Using numerical modeling, we show that these events of methane hydrate instability were possibly triggered by the rapid warming of intermediate waters by ~2.5−3.5 °C in the South China Sea. This finding provides direct evidence for the sensitivity of the deep marine methane hydrate reservoir to glacial-interglacial climatic and oceanographic cyclicity.

1. Introduction

Seafloor methane seepage is a widespread phenomenon at continental margins (Suess, 2020), whereby methane-rich fluids can be derived from the thermal maturation of organic matter at depth (Galimov, 1988), microbial methanogenesis in the sub-surface sediment (Claypool and Kaplan, 1974), and/or the dissociation of methane hydrate (Bohrmann et al., 1998). Globally, about 3–4% of the organic carbon deposited on the seafloor is converted to methane (Egger et al., 2018). At methane seeps, the key biogeochemical process is the anaerobic oxidation of methane (AOM), which is mediated by a consortium of methanotrophic archaea and sulfate-reducing bacteria (Boetius et al., 2000). This microbial activity results in the precipitation of authigenic carbonates close to the seafloor (Peckmann and Thiel, 2004). Additionally, the oxidation of reduced chemical compounds by chemosynthetic microbes at methane seeps supports a large diversity of benthic ecosystems (Boetius and Wenzhöfer, 2013). Although the precipitation of carbonates represents an efficient sink for methane-derived carbon in the sediment, large volumes of methane can be transferred into the water column and even to the atmosphere (Solomon et al., 2009). In the geological past, massive methane releases have occurred episodically at the seafloor in response to the dissociation of methane hydrates (Dickens et al., 1995; Kennett et al., 2000; Dickens, 2003). Methane hydrates are unstable phases, particularly sensitive to temperature and pressure variations (Buffett, 2000). For the Santa Barbara Basin, Kennett et al. (2000) proposed that past changes in intermediate water temperatures led to methane hydrate dissociation and enhanced methane fluxes during the last interstadials, with an impact on the millennial variability of the Late Quaternary climate. While this 'Clathrate Gun Hypothesis' (Kennett et al., 2003) has been subject to much debate over past decades (Wallmann et al., 2018), especially concerning its presumed impact on short-term climate change, recent work has suggested that a major episode of hydrate dissociation occurred

in the South China Sea (SCS) during the last interglacial (Chen et al., 2019), hence providing support for a possible mechanism linking methane seepage to Late Quaternary climate change. Nevertheless, it still remains unclear how methane seeps at marine continental margins may respond to global climate change, especially at the timescale of glacial-interglacial cycles. During the Quaternary, sea-level variations, major changes in deep-ocean temperatures, and organic carbon burial are likely to have influenced seafloor methane emissions (Karstens et al., 2018; Oppo et al., 2020). At the global scale, methane seepage is thought to be primarily enhanced during periods of low sea level (Teichert et al., 2003; Feng et al., 2010; Tong et al., 2013; Han et al., 2014; Oppo et al., 2020; Wang et al., 2022), because reduced hydrostatic pressure can result in the destabilization of methane hydrates stored in the sediment. Tectonic activity and ice sheet dynamics have also been shown to play a role in methane release on glaciated continental margins (Crémière et al., 2016; Wallmann et al., 2018; Himmler et al., 2019). Also, the influence of bottom-water temperature on methane hydrate dissociation and seepage has also been reported (Hill et al., 2006; Deng et al., 2021; Weldeab et al., 2022).

The dating of authigenic carbonates preserved in the sedimentary record can provide a chronology of past methane release events (Teichert et al., 2003; Feng et al., 2010; Tong et al., 2013; Han et al., 2014; Crémière et al., 2016; Chen et al., 2019; Himmler et al., 2019). This is usually achieved by direct dating of seep carbonates using the uranium series, but also through age determination of the host sediments (Oppo et al., 2020). In previous studies, most uranium-thorium (U-Th) investigations have focused on seep carbonates recovered at the seafloor or from meter-long sediment cores, hence providing limited information on the temporal evolution of fluid seepage over longer timescales. This limitation can be overcome when considering longer sedimentary records that span multiple climatic cycles (Himmler et al., 2019). In their recent U-

Th investigation of drilled seep carbonates, Chen et al. (2019) suggested that increased bottom-water temperature during Marine Isotope Stage (MIS) 5e caused methane hydrate destabilization at the SCS margin. This finding provided the first direct evidence that methane seepage likely intensified during full sea-level highstands. Additional investigation of deeply buried seep carbonates is required to assess whether this hypothesis holds true for earlier interglacial episodes, and to further test potential relationships linking both methane hydrate stability and seepage intensity to Late Quaternary climate change.

The SCS is the largest marginal sea of the western Pacific and has an area of active methane seepage (Tong et al., 2013; Han et al., 2014). The northern SCS exchanges intermediate and deep waters from the Pacific through the Luzon Strait, with a sill depth of about 2600 m (Lüdmann et al., 2005). The vertical section of the net flow through the Luzon Strait shows a vertical structure: water enters from the deep layer (>1500 m) into the SCS, and then flows out of the SCS into the Pacific in the intermediate layer (500–1500 m). These water masses are referred to as SCS deep and intermediate waters, respectively. The physical properties of the intermediate water mass in the northern SCS are similar to those of intermediate water of the western North Pacific, with temperatures between 11°C and 3°C and salinities between 34.5 and 34.6 per mil (Wyrtki, 1961). Therefore, the SCS is particularly well-suited to investigate the effect of Late Quaternary intermediate-water circulation changes on long-term methane hydrate instability and related methane seepage at the continental marine margins. Here, we expand the geological history of past methane releases in the SCS to about 440 thousand years BP. Based on U-Th dating of the seep carbonates and age determination of host sediments from drill cores, we show that six out of seven episodes of methane release events during the last 440 thousand years coincided with major interglacials.

2. Materials and Methods

2.1. Sediment core sampling

The samples were collected from three conventional drilling cores by Fugro during the 2nd Gas Hydrate Drilling Expeditions conducted by Guangzhou Marine Geological Survey in the Dongsha (GMGS2–08, GMGS2–09B, GMGS2–16; water depth of 664–871 m) area (Fig. 1).

2.2. Carbonate mineralogy

Semi-quantitative carbonate mineral composition was determined by X-ray powder diffraction (XRD) on bulk powders of representative samples. The analyses were conducted using a BRUKER D8 ADVANCE (Germany) using CuKα radiation at 40 kV and 300 mA. Scans were conducted from 2° to 65° (2θ) with a step size of 0.01° and a count time of 1 s per step. The relative proportions of minerals were semi-quantitatively assessed by way of a Rietveld analysis of the diffractograms using the program JADE 6.0. The measurements were accomplished at Guangzhou Marine Geological Survey.

2.3. Carbon and oxygen stable isotope analysis

Planktonic (*Globigerinoides ruber*) and benthic (*Uvigerina peregrina*) foraminifera tests for carbon and oxygen stable isotope measurements were picked from the > 154 μm size fraction and cleaned according to the standard protocol. The stable isotope compositions of foraminifera and hand-drilled seep carbonates were analyzed at Guangzhou Marine Geological Survey using a Kiel IV online carbonate preparation line connected to a Thermo Finnigan MAT253 mass spectrometer (Thermo Scientific, USA). Isotope compositions are expressed using the δ notation

relative to the Vienna Pee Dee Belemnite (VPDB) standard. The reproducibility is better than ±0.08‰ for both $\delta^{13}C$ and $\delta^{18}O$ values.

2.4. U-Th chronology

Solution multi-collector inductively coupled plasma mass spectrometer (MC-ICP-MS): Samples were selected from two carbonate layers in cores GMGS2–09. Carbonate nodules were discarded because of the high contents of detrital minerals. Sample preparation and measurement were the same as described by Chen et al. (2019). Briefly, measurements were carried out on 10−25 mg micro-drilled carbonate samples (Fig. S2 and Table S4). At Xi'an Jiaotong University, measurements were made on a MC-ICP-MS (Thermo-Finnigan Neptune). Analytical protocols for the separation and purification of U and Th from carbonates and instrument dispositions are the same as those described in Cheng et al. (2013). U decay constants: $\lambda_{238} = 1.55125 \times 10^{-10}$ and $\lambda_{234} = 2.82206 \times 10^{-6}$ (Jaffey et al., 1971; Cheng et al., 2013). Th decay constant: $\lambda_{230} = 9.1705 \times 10^{-6}$ (Cheng et al., 2013). The uncertainties of our age data are quoted at 2σ. $\delta^{234}U = ([^{234}U/^{238}U]_{activity} - 1) \times 1000$. $\delta^{234}U_{initial}$ was calculated based on ^{230}Th age (T), i.e., $\delta^{234}U_{initial} = \delta^{234}U_{measured} \times e^{\lambda 234} \times T$. A $^{230}Th/^{232}Th$ atomic ratio of $4.4 \pm 2.2 \times 10^{-6}$ was used to correct initial ^{230}Th. Those are the values for a material at secular equilibrium, with the bulk earth $^{232}Th/^{238}U$ value of 3.8. The errors are arbitrarily assumed to be 50%.

In-situ laser ablation MC-ICP-MS: The U and Th isotopes of seep carbonate nodules were measured using MC-ICP-MS (Neptune plus) coupled with the New Wave 193HE ArF Excimer laser system at the State Key Laboratory for Mineral Deposits Research, Nanjing University. Retarding Potential Quadrupole (RPQ) mode of the MC-ICP-MS was activated during the analysis to improve the abundance sensitivity. Helium gas was used as the carrier gas and was

mixed with Ar and N_2 before injection into the plasma. Large laser spot size (150 μm) and high repetition (20 Hz) were used to increase the intensity of the signal and line scanning (2 mm) was applied to increase signal stability (Spooner et al., 2016). The NIST 612 glass standard was used to tune the instrumental parameters before the analysis of seep carbonates. An inorganic aragonite vein (VS001/1-A) was used as a bracketing standard to correct the instrumental mass bias of isotopic ratios (Spooner et al., 2016). Such an in-situ dating method has been previously proven to be accurate and reliable for the determination of U-Th isotopes of carbonates, such as corals, seep carbonates, and speleothems (Spooner et al., 2016; Wang et al., 2022). Spooner et al. (2016) provide details regarding data reduction and error estimation. A $^{230}Th/^{232}Th$ atomic ratio of 4.4×10^{-6} with 10% uncertainty was used to correct the initial ^{230}Th (Feng et al., 2010). The applied initial $^{230}Th/^{232}Th$ atomic ratio is representative of the upper continental materials at secular equilibrium with the bulk earth $^{232}Th/^{238}U$ value of 3.8 (Feng et al., 2010).

2.5. TOC, TS, $CaCO_3$ analysis

Total organic carbon (TOC) and total sulfur (TS) were quantified using a Heraeus CHN-O Rapid elemental analyzer. For TOC measurements, 10% HCl was added to remove carbonate before analysis. Carbonate content was analyzed using the EDTA (Ethylene diamine tetraacetic acid) method. The precision and accuracy of the TOC, TS, and $CaCO_3$ values were better than 3%.

2.6. Major and trace element analysis

Major elements (Al, Mn, Fe) were analyzed using an X-Ray Fluorescence Spectrometer (Axios PW4400/40, PANalytical, Netherlands). Trace elements (Mo, U, V, Cu, Ni, Co, Zn, Zr,

Rb) analysis was performed using HF-HNO_3 solutions according to the method established by Liang et al. (2017). Trace elements were measured via ICP-mass spectrometry (MS) (X Series2, Thermo Fisher Scientific, Waltham, MA, USA) at Guangzhou Marine Geological Survey. The precision and accuracy of these values were better than 5% for Al, Mn, Fe, U, V, Cu, Ni, Co, Zn, Zr, Rb, and 10% for Mo.

2.7. AMS 14C chronology

Two AMS ^{14}C measurements were made on planktonic foraminifera tests (*Globigerinoides sacculifer*) collected from core GMGS2–16. Pretreatment, preparation, and measurement were conducted by Beta Analytic Inc. (Miami, FL, USA). Dates were calibrated by Beta Analytic Inc. and reported to the 2 sigma range.

2.8. Methane hydrate stability diagram

CSMHYD software was used to predict methane hydrate stability under the assumed conditions (Sloan, 1998). This method illustrates changes in the stability of methane hydrates and does not consider the transient behavior of the system and methane solubility. We used the present bottom water temperature of 5.4 ºC for core GMGS2–16 from the Dongsha area; the gas compositions are 100% methane (Zhang et al., 2015). The geothermal gradient at coring site GMGS2–16 is 41 ºC km^{-1} (Feng et al., 2015). Sea-level and bottom water temperature records during the Last Glacial Maximum (LGM) and 105 to 140 ka are those determined for ODP1123 (Elderfield et al., 2012; Bates et al., 2014).

3. Results

3.1.Stratigraphy of carbonate layers and nodules

Drill cores GMGS2–08 (water depth of 801 m), GMGS2–09B (water depth of 664 m), and GMGS2–16 (water depth of 871 m) from the Dongsha area reached maximum depths of 93.84 m, 30.00 m, and 213.55 m, respectively. The cores are mainly composed of hemipelagic sediment dominated by clay. Authigenic carbonates occur either as nodules or as crusts (Fig. 1b and Figs. S2, S3, S4). Carbonate crusts occur as fillings that formed 0.5 to 1.0 centimeter pores inside impure early-generation cement, mud, and early-generation carbonate cemented sediments. Carbonate nodules are mainly composed of micrite cementing fine-grained terrigenous sediment. Nodules represent the only type of authigenic carbonates in core GMGS2–16, whereas both nodules and crusts are encountered in the other three cores (Fig. 1b). Massive carbonate crusts up to 1 m thick were identified in core GMGS2–08F from 58.95 to 59.46 mbsf (meters below seafloor) and 61.52 to 62.55 mbsf, respectively. Two thinner carbonate crusts (~5 cm-thick) were observed in core GMGS2–09B from 6.20 to 6.45 mbsf and 22.20 to 22.60 mbsf, respectively. Bivalve shells were abundant in all studied cores. All shells were scattered throughout the sediment rather than being cemented within seep carbonates. Direct dating of these shells was not attempted in this study.

3.2. Mineralogy and carbon-oxygen isotope composition of seep carbonates

Aragonite is the dominant carbonate phase in all carbonate crusts (40–100% with an average of 64%; Table S1). Carbonate nodules from the Dongsha area are mostly composed of high-Mg calcite. The $\delta^{13}C$ values ranged from −62.3‰ to −38.9‰ (mean value ± 1σ: −49.7 ± 4.5‰; n = 143) for the seep carbonates (Fig. 2; Table S2), while $\delta^{18}O$ values ranged between 2.3‰ and 6.0‰ (4.0 ± 0.6‰; n = 143) (Fig. 2; Table S2). There is no significant difference in

carbon and oxygen isotope composition between the microcrystalline matrix and the fibrous cement (Table S2).

3.3. Carbon and oxygen isotopes in planktonic and benthic foraminifera

The $\delta^{13}C$ and $\delta^{18}O$ values ranged from −5.4‰ to 0.1‰ and from 2.7‰ to 4.1‰ (n = 154) for benthic species (*Uvigerina peregrina*) and from −8.4‰ to 1.9‰ and −3.5‰ to −0.4‰ (n=1471) for planktonic species (*Globigerinoides ruber*; Fig. 3; Table S3). The $\delta^{13}C$ values of most planktonic and benthic foraminifera from the depth intervals between 3.50 to 10.50 mbsf and 191.06 to 195.76 mbsf were significantly lower than those encountered at other SCS sites in Late Quaternary hemipelagic sediment sequences unaffected by seepage (Fig. 3; Jian et al., 2003). Note that the $\delta^{18}O$ depth profile for foraminifera from the above intervals displays an opposite trend to $\delta^{13}C$ values. Most likely, the relatively negative $\delta^{13}C$ values measured for both planktonic and benthic foraminifera at the study sites reflect diagenetic overprinting by authigenic carbonate minerals having strongly negative $\delta^{13}C$ signatures (Panieri et al., 2017).

3.4. Age constraints on carbonate formation

Uranium-thorium dating was carried out on crust samples collected from one distinct carbonate layer from core GMGS2–09 at depths from 6.20 to 22.60 m (Fig. S2 and Table S4). Uranium concentrations and $\delta^{234}U$ values for these samples ranged from 3.1 to 10.7 μg/g and 134 to 148‰, respectively. The studied carbonate samples from cores GMGS2–09 yielded age ranges between ca. 9 to 16 ka (mean age, ~13 ka; n = 8; Table S4). As shown previously (Teichert et al., 2003), U-Th dating of carbonate nodules is often complicated by both low U concentrations and the abundant presence of detrital minerals. In this study, dating of these

samples was attempted using in-situ laser ablation MC-ICP-MS (Figs. S3, S4, and Table S5). The carbonate samples from cores GMGS2–08E at a depth of 58.81 to 66.54 m yielded age ranges between approximately 108 to 137 ka (mean age, ~125 ka; n = 5). The carbonate samples from cores GMGS2–08B in the upper 3.7 m yielded age ranges of ca. 7 to 10 ka (mean age, ~8 ka; n = 3; Table S6).

A more direct approach for dating seep carbonate layers is to determine the age of the associated sediments (Oppo et al., 2020). This was conducted for core GMGS2–16 by establishing a robust depth-age model, using foraminifera ^{14}C dates (Table 1) and sediment biostratigraphic ages (Chen et al., 2016b). The sediment Zr/Rb and Mn/Fe ratios were correlated and tuned to the relative sea level change of ODP1143 records (Bates et al., 2014), and followed by tuning the resulting planktonic $\delta^{18}O$ curve to the LR04 (Lisiecki and Raymo, 2005) and ODP1146 (Clemens et al., 2008) stacked records (Figs. 4, 5).

The presence of seep carbonate accompanied by molybdenum (Mo) enrichments in host sediments represents a reliable indicator of past intense methane seepage (Chen et al., 2016c). Molybdenum, as dissolved molybdate, behaves is conservative in oxic seawater. In the presence of hydrogen sulfide, the formation of thiomolybdates is scavenged by iron sulfides and organic materials and removed from the aqueous phase (Erickson and Helz, 2000). Sedimentary Mo enrichments have been used to constrain the redox conditions in the water column and sediment; both anaerobic oxidation of methane and organoclastic sulfate reduction can produce the hydrogen sulfide. In core GMGS2–16, significant Mo and total sulfur (TS) enrichments are encountered in the sediment associated with authigenic carbonate layers (Fig. 6). In the absence of high TOC content and any other enrichment of other redox-sensitive elements (V, Ni, Cu, Zn, Co; Table S7), these enrichments are best interpreted to result from anaerobic oxidation of

methane (Chen et al., 2016c). In such cases, sediments bearing seep carbonate and typified by molybdenum (Mo) enrichments can be expected to provide constraints on the timing of seepage (Chen et al., 2016c). Using this approach, the seep carbonate layers with Mo enrichment (Mo_{EF}>5) in core GMGS2–16 were dated as follows: ca. 2 to 8 ka, ca. 235 ka, ca. 303 ka, ca. 329 ka, ca. 419 to 423 ka, and ca. 432 to 436 ka (Figs. 6, 7a and Table S6).

4. Discussion

4.1. Seep carbonates record the dissociation of methane hydrates

Overall, the negative carbon isotopic compositions of the studied authigenic carbonates are similar to other seep carbonates, thus producing strong support that the dissolved inorganic carbon is mainly derived from methane oxidation (Peckmann and Thiel, 2004). The presence of strongly ^{13}C-depleted carbonates ($\delta^{13}C < -45‰$) in the studied samples indicates that the main carbon source was biogenic methane, which is more ^{13}C depleted than thermogenic methane (Schoell, 1980). Furthermore, the observed $\delta^{13}C_{carbonate}$ and $\delta^{13}C_{methane}$ values (Zhang et al., 2015) also clearly indicate a biogenic origin for methane in the Dongsha area.

The $\delta^{18}O$ composition of seep carbonates is largely inherited from the fluid source but is also dependent on temperature during precipitation (Bohrmann et al., 1998). Paleotemperature calculations (Kim et al., 2007) using a seawater $\delta^{18}O$ value of −0.3‰ (VSMOW; Feng and Chen, 2015) result in an unrealistic estimate ranging from −3.8 to −1.8 ºC, which is significantly colder than modern bottom water temperature in the Dongsha areas (5.4 ºC; *in situ* tests). When using the seawater $\delta^{18}O$ value of 0.8‰ (VSMOW), reflecting changes in the bottom water $\delta^{18}O$ associated with sea level oscillations, and present-day bottom water temperatures to calculate equilibrium $\delta^{18}O$, the values of aragonite are about 3.5‰. Such value is significantly lower than most of the $\delta^{18}O$ values measured in the seep carbonates ($2.3‰ < \delta^{18}O < 6.0‰$; Fig. 2). This

finding reflects the influence of ^{18}O-enriched fluids on carbonate formation (Fig. 2), which could reflect either clay mineral dehydration in the deeper sediment column (Hensen et al., 2004) or dissociation of methane hydrates (Bohrmann et al., 1998). Considering the ubiquitous distribution of methane hydrate at the study sites, the high $\delta^{18}O$ values (as high as 6.0‰; Fig. 2) of seep carbonates are consistent with local methane hydrate dissociation.

4.2. Interglacial-glacial cyclicity influences marine methane hydrate stability

Considering the new results and using different dating methods in combination with previous observations from younger seafloor seep carbonates associated with SCS active seeps (Site F; ~2 to 11 ka; Feng and Chen, 2015) and buried carbonate nodules from core GMGS2–08E, GMGS2–08F at depths of about 61 m (~113 to 133 ka; Chen et al., 2019; Deng et al., 2021; Table S6), our new data, in combination with the previous investigations, demonstrate synchronicity between the intervals of intensified methane seepage and the last major interglacial episodes of the Late Quaternary: that is MIS 1 (~2 to 16 ka), 5e (~114 to 132 ka), 7c (~236 to 248 ka), 9c (~303 to 337 ka), and 11c (~384 to 422 ka; Figs. 7a). Furthermore, we identify an additional methane release event, which appears to correspond to a local sea-level lowstand (~432 to 436 ka).

In the marine environment, methane hydrates are stable at relatively high hydrostatic pressure and low temperature conditions (Buffett, 2000). Consequently, any significant rise in bottom water temperature and/or sea level fall may result in methane hydrate destabilization from the top of the gas hydrate stability zone (GHSZ; Ruppel and Kessler, 2017). Previous investigations have suggested that extensive methane hydrate dissociation was favored during glacial periods in response to lower-pressures associated glacio-eustatic sea level fall (Teichert et

al., 2003). However, numerical simulations suggest that the impact of sea level change on the thinning of the GHSZ during glacials could readily be compensated by bottom water cooling (Ruppel and Kessler, 2017). Nevertheless, the evidence for active methane seepage during ca. 432–436 ka at site GMGS2−16 could possibly have resulted from an episode of hydrate dissociation caused by sea level fall. However, in this case, neither seep carbonate nor sedimentary Mo enrichment are evident in core GMGS2–16 during MIS 5e, suggesting that methane seepage was less intense at this location compared to the other cores (Fig. 1a). This interpretation is consistent with the mineralogy of seep carbonates in this core. The dominance of high-Mg calcite among the seep carbonates likely indicates precipitation under relatively low methane flux and more restricted, reducing conditions. In contrast, aragonite precipitation is favored under conditions of strong seepage typified by the formation of methane bubbles (Aloisi et al., 2002).

The ages we assign to the formation of seep carbonates in sequences of SCS margin, in combination with evidence for positive $\delta^{18}O$ signatures (> 4‰ VPDB), suggest that major episodes of methane hydrate dissociation took place during each of the last interglacial episodes. The dissociation of hydrate provided both dissolved inorganic carbon and ^{18}O-enriched waters during the precipitation of seep carbonates. The presence of recurrent methane release events during interglacials over the last 440,000 years, found in the Dongsha area, calls for an external forcing mechanism that affected the methane hydrate reservoir during sea-level highstands. Potential triggers for enhanced methane seepage during the warmer interglacial episodes include variations in local sedimentation rates, mass wasting processes, glacial tectonics induced by ice sheet dynamics, and bottom water warming (Kennett et al., 2000; Hill et al., 2006; Karstens et al., 2018; Himmler et al., 2019). Rapid sedimentation caused temperature reequilibration in the

sediment's column that triggered methane hydrate dissociation near the end of the last glaciation in the margin off Norway (Karstens et al., 2018). However, the sedimentation rate in the SCS areas did not exceed 1 m/ka, which is significantly lower than rates for the Norwegian margin (> 8 m/ka; Karstens et al., 2018). Since the carbonates from the Dongsha area were all sampled on ridge crests (Fig. 1a), mass wasting processes were unlikely to be the primary cause affecting local methane hydrate stability. Any effect induced by ice sheet fluctuations on methane seepage is confined to glaciated areas. Other driving mechanisms proposed to explain past episodes of methane hydrate destabilization include increased heat flow, reduced hydrostatic pressure, regional decrease in methane concentration, or changes in pore water salinity (Hensen et al., 2004; Ruppel and Kessler, 2017). However, for the SCS margin, none of these factors are likely to have been important in affecting methane hydrate stability during the Quaternary. Thus water mass temperature change represents the most plausible explanation for the episodic release of hydrate-bound methane during interglacials.

Numerous observational and modeling studies have indicated that methane hydrates within upper continental slope sediments can disassociate during ocean warming. As such, the stability of gas hydrate can be affected even by small changes in intermediate water temperature (e.g., Kennett et al., 2003; Westbrook et al., 2009; Phrampus and Hornbach, 2012; Phrampus et al., 2014; Berndt et al., 2014; Brothers et al., 2014; Skarke et al., 2014; Ruppel and Kessler, 2017), a concept previously emphasized by Kennett et al. (2003) in the 'Clathrate Gun Hypothesis'. Seabed warming may therefore increase the methane release from the seabed through the reduction of the extent of the GHSZ. This increased methane release from hydrate dissociation was observed in the Santa Barbara Basin, the North Atlantic, the Arctic Ocean, and

other high-latitude shallow seas (Kennett et al., 2000; Hill et al., 2006; Westbrook et al., 2009; Phrampus and Hornbach, 2012; Ruppel and Kessler, 2017).

The sediment sequences investigated are from the upper continental slope and influenced by North Pacific Intermediate Water. During the last five interglacials, peak temperatures of intermediate waters in the northern SCS rose by approximately 2.5 to 3.5 ºC (Fig. 7b; see Supplementary Material). Numerical modeling indicates that during the last glacial maximum large volumes of methane hydrates formed in response to low bottom-water temperature, resulting in the thickening of the GHSZ (Fig. 8a). Following deglaciation, warm Pacific waters flowed into the SCS. This caused a 2.5 to 3.5 ºC increase in bottom water temperatures on the SCS margin in less than five thousand years. The increased temperature reduced the extent of the GHSZ and triggering methane hydrate dissociation (Fig. 8a). This same hydrate dissociation state also took place in intervals between 105 to 140 ka (Fig. 8b).

5. Conclusions and implications

Based on our studies of authigenic carbonate crusts from the Dongsha area of the South China Sea (SCS), we consider that increased temperature of intermediate water masses at the onset of interglacial episodes was the primary driver of intensified methane seepage in the SCS. This study provides the first direct evidence that methane seepage was repeatedly triggered when deep intermediate Pacific waters warmed during interglacial episodes. This study is likely to stimulate further similar investigation in other parts of the world ocean, since it may have significant implications for the history of climatic change. The same chain of events is likely to have occurred elsewhere along the world's continental margins, related to re-organization of intermediate water circulation during glacial/interglacial oscillations. Evidence for a 2 ºC temperature increase has been reported for intermediate waters along the western North Atlantic

margin over glacial/interglacial cycles (Dwyer et al., 2000), while an even greater temperature increase of 3 ºC has been reported for the Southwest Pacific margin (Elmore et al., 2015).

Currently, there is little knowledge and understanding globally about methane seepage change in the past. Nevertheless, this work suggests that if similar processes as those identified for the SCS occur widely on continental margins, the climate change-induced hydrate dissociation will become an important source of methane to the ocean, as evidenced by previous studies for the Southern California margin (Hill et al., 2006). The impact of deep/intermediate water warming on methane hydrate stability needs to be considered in the context of future ocean warming (Weldeab et al., 2022), since major methane release from destabilizing hydrates into the water column can potentially increase ocean acidity, decrease dissolved oxygen, affect the marine carbon cycle, and serve as a feedback for climate change.

Declaration of Competing Interest

The authors declare no conflicts of interest relevant to this study.

Acknowledgments

We thank the crew and scientists of the research vessels of the GMGS2 gas hydrate drilling expeditions. S. Wan (SCSIO, CAS) is acknowledged for helpful discussion. Y. Cao (SHOU) is thanked for his help during methane hydrate modeling. Funding was provided by the NSF of China (Grants: 42225603, 41976061), the development fund of South China Sea Institute of Oceanology of the Chinese Academy of Sciences (SCSIO202202), and the Program of Guangdong Basic and Applied Research (Grant: 2019B030302004). Science editor Wenjiao

Xiao, associate editor Ganqing Jiang, reviewers James Kennett and Yinan Deng are thanked for helpful comments that helped to improve the manuscript.

Author contributions

The study was designed by D.F. and N.L. J.F. and F.C. prepared the samples. N.L., J.F., Y.Z., X.W., and D.C. performed XRD measurements and stable isotope analyses. N.L. conducted U-Th dating with input from M.W., T.C., H.C. and R.L.E. N.L., D.F., J.P., G.B. led data interpretation and developed the manuscript. All authors contributed to discussion and manuscript revision.

Appendix A. Supplementary data

Supplementary materials to this article can be found online at xx.

References

Aloisi, G., Bouloubassi, I., Heijs, S.K., Pancost, R.D., Pierre, C., Sinninghe Damsté, J.S., Gottschal, J.C., Forney, L.J., and Rouchy, J.M., 2002, CH_4-consuming microorganisms and the formation of carbonate crusts at cold seeps: Earth and Planetary Science Letters, v. 203, p. 195–203, https://doi.org/10.1016/S0012-821X(02)00878-6.

Bates, S.L., Siddall, M., and Waelbroeck, C., 2014, Hydrographic variations in deep ocean temperature over the mid-Pleistocene transition: Quaternary Science Reviews, v. 88, p. 147−158, https://doi.org/10.1016/j.quascirev.2014.01.020.

Berndt, C., Feseker, T., Treude, T., Krastel, S., Liebetrau, V., Niemann, H., Bertics, V.J., Dumke, I., Dünnbier, K., Ferré, B., Graves, C., Gross, F., Hissmann, K., Hühnerbach, V., Krause, S., Lieser, K., Schauer, J., Steinle, L., 2014, Temporal constraints on hydrate-

controlled methane seepage off Svalbard: Science, v. 343, p. 284–287, https://doi.org/10.1126/science.1246298.

Boetius, A., Ravenschlag, K., Schubert, C.J., Rickert, D., Widdel, F., Gieseke, A., Amann, R., Jørgensen, B.B., Witte, U., and Pfannkuche, O., 2000, A marine microbial consortium apparently mediating anaerobic oxidation of methane: Nature, v. 407, p. 623–626, https://doi.org/10.1038/35036572.

Boetius, A., and Wenzhöfer, F., 2013, Seafloor oxygen consumption fuelled by methane from cold seeps: Nature Geoscience, v. 6, p. 725−734, https://doi.org/10.1038/ngeo1926.

Bohrmann, G., Greinert, J., Suess, E., and Torres, M., 1998, Authigenic carbonates from the Cascadia subduction zone and their relation to gas hydrate stability: Geology, v. 26, p. 647–650, https://doi.org/10.1130/0091-7613(1998)026<0647:ACFTCS>2.3.CO;2.

Brothers, D.S., Ruppel, C., Kluesner, J.W., ten Brink, U.S., Chaytor, J.D., Hill, J.C., Andrews, B.D., and Flores, C., 2014, Seabed fluid expulsion along the upper slope and outer shelf of the U.S. Atlantic continental margin: Geophysical Research Letters, v. 41, p. 96–101, https://doi.org/10.1002/2013GL058048.

Buffett, B.A., 2000, Clathrate hydrates: Annual Review of Earth and Planetary Sciences, v. 28, p. 477−507, https://doi.org/10.1146/annurev.earth.28.1.477.

Chen, F., Lu, H.F., Liu, J., Zhuang, C., Wu, C., Cao, J., Zhou, Y., and Liu, G.H., 2016a, Sedimentary geochemical response to gas hydrate episodic release on the northeastern slope of the South China Sea: Earth Science, v. 41, p. 1619–1629 (in Chinese with English abstract), https://doi: 10.3799/dqkx.2016.120.

Chen, F., Zhuang, C., Zhou, Y., Su, X., Duan, X., Liu, G., Wu, C., and Jing, X., 2016b, Calcareous nannofossils and foraminifera biostratigraphy on the northeastern slope of the

South China Sea and variation in sedimentation rates: Earth Science, v. 41, p. 416−424 (in Chinese with English abstract), https:// doi: 10.3799/dqkx.2016.033.

Chen, F., Hu, Y., Feng, D., Zhang, X., Cheng, S.H., Cao, J., Lu, H.F., and Chen, D.F., 2016c, Evidence of intense methane seepages from molybdenum enrichments in gas hydrate-bearing sediments of the northern South China Sea: Chemical Geology, v. 443, p. 173−181, https://doi.org/10.1016/j.chemgeo.2016.09.029.

Chen, F., Wang, X.D., Li, N., Cao, J., Bayon, G., Peckmann, J., Hu, Y., Gong, S.G., Chene, H., Edwards, L., Ning, Y.F., Jin, M., Huang, H.W., Wu, C., Sun, Y.D., Chen, H., Zhou, Y., Chen, D.F., and Feng, D., 2019, Gas hydrate dissociation during sea-level highstand inferred from U/Th dating of seep carbonate from the South China Sea: Geophysical Research Letters, v. 46, p. 13928−13938, https://doi.org/10.1029/2019GL085643.

Cheng, H., Edwards, R.L., Shen, C.C., Polyak, V.J., Asmerom, Y., Woodhead, J., Hellstrom, J., Wang, Y.J., Kong, X.G., Spotl, C., Wang, X.F., and Alexander, E.C., 2013, Improvements in ^{230}Th dating, ^{230}Th and ^{234}U half-life values, and U-Th isotopic measurements by multi-collector inductively coupled plasma mass spectrometry: Earth and Planetary Science Letters, v. 82−91, p. 371−372, https://doi.org/10.1016/j.epsl.2013.04.006.

Claypool, G.E., and Kaplan, I.R., 1974, The origin and distribution of methane in marine sediments. Kaplan (Ed), Natural Gases in Marine Sediments, Plenum Publishing Corp, New York, 99–139.

Clemens, S.C., Prell, W.L., Sun, Y.B., Liu, Z.Y., and Chen, G.S., 2008, Southern Hemisphere forcing of Pliocene delta O-18 and the evolution of Indo-Asian monsoons: Paleoceanography, v. 23, https://doi.org/10.1029/2008PA001638.

Crémière, A., Lepland, A., Chand, S., Sahy, D., Condon, D.J., Noble, S.R., Martma, T., Thorsnes, T., Sauer, S., and Brunstad, H., 2016, Timescales of methane seepage on the Norwegian margin following collapse of the Scandinavian Ice Sheet: Nature Communications, v. 7, 11509, https://doi.org/10.1038/ncomms11509.

Deng, Y.N., Chen, F., Li, N., Jin, M., Cao, J., Chen, H., Zhou, Y., Wu, C., Zhuang, C., Zhao, Y., and Cheng, S.H., 2019, Cold-water corals in gas hydrate drilling cores from the South China Sea: Occurrences, geochemical characteristics and their relationship to methane seepages: Minerals, v. 9, 742, https://doi.org/10.3390/min9120742.

Deng, Y., Chen, F., Guo, Q., Hu, Y., Chen, D., Yang, S., Cao, J., Chen, H., Wei, R., Cheng, S., Zhou, J., Liu, C., Jiang, X., and Zhu J., 2021, Possible links between methane seepages and glacial-interglacial transitions in the South China Sea: Geophysical Research Letters, v. 48, e2020GL091429, https://doi.org/10.1029/2020GL091429.

Dickens, G.R., Oneil, J.R., Rea, D.K., and Owen, R.M., 1995, Dissociation of oceanic methane hydrate as a cause of the carbon-isotope excursion at the end of the Paleocene: Paleoceanography, v. 10, p. 965−971, https://doi.org/10.1029/95PA02087.

Dickens, G.R., 2003, Rethinking the global carbon cycle with a large, dynamic and microbially mediated gas hydrate capacitor: Earth and Planetary Science Letters, v. 213, p. 169−183, https://doi.org/10.1016/S0012-821X(03)00325-X.

Dwyer, G.S., Cronin, T.M., Baker, P.A., and Rodriguez-Lazaro, J., 2000, Changes in North Atlantic deep-sea temperature during climate fluctuations of the last 25,000 years based on ostracode Mg/Ca ratios: Geochemistry, Geophysics, Geosystems, v. 1, https://doi.org/10.1029/2000GC000046.

Egger, M., Riedinger, N., Mogollon, J.M., and Jørgensen, B.B., 2018, Global diffusive fluxes of methane in marine sediments: Nature Geoscience, v. 11, p. 421–425, https://doi.org/10.1038/s41561-018-0122-8.

Elderfield, H., Ferretti, P., Greaves, M., Crowhurst, S., McCave, I.N., Hodell, D., and Piotrowski, A.M., 2012, Evolution of ocean temperature and ice volume through the mid-Pleistocene climate transition: Science, v. 337, p. 704−709, https://doi.org/10.1126/science.1221294.

Elmore, A.C., McClymont, E.L., Elderfield, H., Kender, S., Cook, M.R., Leng, M.J., Greaves, M., and Misra, S., 2015, Antarctic Intermediate Water properties since 400 ka recorded in infaunal (*Uvigerina peregrina*) and epifaunal (*Planulina wuellerstorfi*) benthic foraminifera: Earth and Planetary Science Letters, v. 428, p. 193−203, https://doi.org/10.1016/j.epsl.2015.07.013.

Erickson, B.E., and Helz, G.R., 2000, Molybdenum(VI) speciation in sulfidic waters: Stability and lability of thiomolybdates: Geochimica et Cosmochimica Acta, v. 64, p. 1149–1158, https://doi.org/10.1016/S0016-7037(99)00423-8.

Feng, D., Roberts, H.H., Cheng, H., Peckmann, J., Bohrmann, G., Edwards, R.L., and Chen, D.F., 2010, U/Th dating of cold-seep carbonates: An initial comparison: Deep-Sea Research Part II: Topical Studies in Oceanography, v. 57, p. 2055−2060, https://doi.org/10.1016/j.dsr2.2010.09.004.

Feng, D., and Chen, D.F., 2015, Authigenic carbonates from an active cold seep of the northern South China Sea: New insights into fluid sources and past seepage activity: Deep-Sea Research Part II: Topical Studies in Oceanography, v. 122, p. 74−83, https://doi.org/10.1016/j.dsr2.2015.02.003.

Feng, J.C., Wang, Y., Li, X.S., Li, G., Zhang, Y., and Chen, Z.Y., 2015, Production performance of gas hydrate accumulation at the GMGS2–Site 16 of the Pearl River Mouth Basin in the South China Sea: Journal of Natural Gas Science and Engineering, v. 27, p. 306−320, https://doi.org/10.1016/j.jngse.2015.08.071.

Galimov, E.M., 1988, Sources and mechanisms of formation of gaseous hydrocarbons in sedimentary rocks: Chemical Geology, v. 71, p. 77−95, https://doi.org/10.1016/0009-2541(88)90107-6.

Han, X.Q., Suess, E., Liebetrau, V., Eisenhauer, A., and Huang, Y.Y., 2014, Past methane release events and environmental conditions at the upper continental slope of the South China Sea: constraints by seep carbonates: International Journal of Earth Sciences, v. 103, p. 1873−1887, https://doi.org/10.1007/s00531-014-1018-5.

Hensen, C., Wallmann, K., Schmidt, M., Ranero, C.R., and Suess, E., 2004, Fluid expulsion related to mud extrusion off Costa Rica - A window to the subducting slab: Geology, v. 32, p. 201−204, https://doi.org/10.1130/G20119.1.

Hill, T.M., Kennett, J.P., Valentine, D.L., Yang, Z., Reddy, C.M., Nelson, R.K., Behl, R.J., Robert, C., and Beaufort, L., 2006, Climatically driven emissions of hydrocarbons from marine sediments during deglaciation: Proceedings of the National Academy of Sciences of the United States of America, v. 103, p. 13570−13574, https://doi.org/10.1073/pnas.0601304103.

Himmler, T., Sahy, D., Martma, T., Bohrmann, G., Plaza-Faverola, A., Bunz, S., Condon, D.J., Knies, J., and Lepland, A., 2019, A 160,000-year-old history of tectonically controlled methane seepage in the Arctic: Science Advances, v. 5, eaaw1450, https://doi.org/10.1126/sciadv.aaw1450.

Jaffey, A.H., Flynn, K.F., Glendenin, L.E., Bentley, W.C., and Essling, A.M., 1971, Precision measurement of half-lives and specific activities of ^{235}U and ^{238}U: Physical Review C, v. 4, p. 1889−1906, https://doi.org/10.1103/PhysRevC.4.1889.

Jian, Z.M., Zhao, Q.H., Cheng, X.R., Wang, J.L., Wang, P.X., and Su, X., 2003, Pliocene-Pleistocene stable isotope and paleoceanographic changes in the northern South China Sea: Palaeogeography, Palaeoclimatology, Palaeoecology, v. 193, p. 425−442, https://doi.org/10.1016/S0031-0182(03)00259-1.

Karstens, J., Haflidason, H., Becker, L.W.M., Berndt, C., Rupke, L., Planke, S., Liebetrau, V., Schmidt, M., and Mienert, J., 2018, Glacigenic sedimentation pulses triggered post-glacial gas hydrate dissociation: Nature Communications, v. 9, 635, https://doi.org/10.1038/s41467-018-03043-z.

Kennett, J.P., Cannariato, K.G., Hendy, I.L., and Behl, R.J., 2000, Carbon isotopic evidence for methane hydrate instability during quaternary interstadials: Science, v. 288, p. 128−133, https://doi.org/10.1126/science.288.5463.128.

Kennett, J.P., Cannariato, K.G., Hendy, I.L., and Behl, R.J., 2003, Methane Hydrates in Quaternary Climate Change: The Clathrate Gun Hypothesis, pp. 216, AGU, Washington, D. C

Kim, S.T., O'Neil, J.R., Hillaire-Marcel, C., and Mucci, A., 2007, Oxygen isotope fractionation between synthetic aragonite and water: Influence of temperature and Mg^{2+} concentration: Geochimica et Cosmochimica Acta, v. 71, p. 4704−4715, https://doi.org/10.1016/j.gca.2007.04.019.

Kim, S.T., and O'Neil, J.R., 1997, Equilibrium and nonequilibrium oxygen isotope effects in synthetic carbonates: Geochimica et Cosmochimica Acta, v. 61, p. 3461−3475, https://doi.org/10.1016/S0016-7037(97)00169-5.

Kubota, Y., Kimoto, K., Itaki, T., Yokoyama, Y., Miyairi, Y., and Matsuzaki, H., 2015, Bottom water variability in the subtropical northwestern Pacific from 26 kyr BP to present based on Mg / Ca and stable carbon and oxygen isotopes of benthic foraminifera: Climate of the Past, v. 11, p. 803–824, https://doi.org/10.5194/cp-11-803-2015.

Liang, Q.Y., Hu, Y., Feng, D., Peckmann, J., Chen, L.Y., Yang, S.X., Liang, J.Q., Tao, J., and Chen, D.F., 2017, Authigenic carbonates from newly discovered active cold seeps on the northwestern slope of the South China Sea: Constraints on fluid sources, formation environments, and seepage dynamics: Deep-Sea Research Part I: Oceanographic Research Papers, v. 124, p. 31−41, https://doi.org/10.1016/j.dsr.2017.04.015.

Lisiecki, L.E., and Raymo, M.E., 2005, A Pliocene-Pleistocene stack of 57 globally distributed benthic delta O-18 records: Paleoceanography, v. 20, https://doi.org/10.1029/2004PA001071.

Lüdmann, T., Wong, HK., and Berglar, K., 2005, Upward flow of North Pacific Deep Water in the northern South China Sea as deduced from the occurrence of drift sediments: Geophysical Research Letters, v. 32, L05614, https://doi.org/10.1029/2004GL021967.

Oppo, D., De Siena, L., and Kemp, DB., 2020, A record of seafloor methane seepage across the last 150 million years: Scientific Reports, v. 10, 2562, https://doi.org/10.1038/s41598-020-59431-3.

Panieri, G., Lepland, A., Whitehouse, M.J., Wirth, R., Raanes, M.P., James, R.H., Graves, C.A., Crémière, A., and Schneider, A., 2017, Diagenetic Mg-calcite overgrowths on foraminiferal

tests in the vicinity of methane seeps: Earth and Planetary Science Letters, v. 458, p. 203−212, https://doi.org/10.1016/j.epsl.2016.10.024.

Peckmann, J., and Thiel, V., 2004, Carbon cycling at ancient methane-seeps: Chemical Geology, v. 205, p. 443−467, https://doi.org/10.1016/j.chemgeo.2003.12.025.

Phrampus, B.J., and Hornbach, M.J., 2012, Recent changes to the Gulf Stream causing widespread gas hydrate destabilization: Nature, v. 490, p. 527−530, https://doi.org/10.1038/nature11528.

Phrampus, B.J., Hornbach, M.J., Ruppel, C.D., and Hart P.E., 2014, Widespread gas hydrate instability on the upper U.S. Beaufort margin: Journal of Geophysical Research-Solid Earth, v. 119, p. 8594–8609, https://doi.org/10.1002/2014JB011290.

Reimer, P.J., Bard, E., Bayliss, A., Beck, J.W., Blackwell, P.G., Ramsey, C.B., Buck, C.E., Cheng, H., Edwards, R.L., Friedrich, M., Grootes, P.M., Guilderson, T.P., Haflidason, H., Hajdas, I., Hatte, C., Heaton, T.J., Hoffmann, D.L., Hogg, A.G., Hughen, K.A., Kaiser, K.F., Kromer, B., Manning, S.W., Niu, M., Reimer, R.W., Richards, D.A., Scott, E.M., Southon, J.R., Staff, R.A., Turney, C.S.M., and van der Plicht, J., 2013, Intcal13 and marine13 radiocarbon age calibration curves 0-50,000 years Cal Bp: Radiocarbon, v. 55, p. 1869−1887, https://doi.org/10.2458/azu_js_rc.55.16947.

Ruppel, C.D., and Kessler, J.D., 2017, The interaction of climate change and methane hydrates: Reviews of Geophysics, v. 55, p. 126–168, https://doi.org/10.1002/2016RG000534.

Schoell, M., 1980, The hydrogen and carbon isotopic composition of methane from natural gases of various origins: Geochimica et Cosmochimica Acta, v. 44, p. 649–661, https://doi.org/10.1016/0016-7037(80)90155-6.

Skarke, A., Ruppel, C., Kodis, M., Brothers, D., and Lobecker, E., 2014, Widespread methane leakage from the sea floor on the northern US Atlantic margin: Nature Geoscience, v. 7, p. 657–661, https://doi.org/10.1038/ngeo2232.

Sloan, E.D., 1998, Clathrate Hydrates of Natural Gases, second ed. Marcel Dekker, New York.

Solomon, E.A., Kastner, M., MacDonald, I.R., and Leifer, I., 2009, Considerable methane fluxes to the atmosphere from hydrocarbon seeps in the Gulf of Mexico: Nature Geoscience, v. 2, p. 561–565, https://doi.org/10.1038/ngeo574.

Spooner, P.T., Chen, T.Y., Robinson, L.F., and Coath, C.D., 2016, Rapid uranium-series age screening of carbonates by laser ablation mass spectrometry: Quaternary Geochronology, v. 31, p. 28−39, https://doi.org/10.1016/j.quageo.2015.10.004.

Stuiver, M., and Reimer, P.J, 1993, Extended ^{14}C data base and revised calib 3.0 ^{14}C age calibration program: Radiocarbon, v. 35, p. 215−230, https://doi.org/10.1017/S0033822200013904.

Suess, E., 2020, Marine cold seeps: background and recent advances, *in* Wilkes, H., ed., Hydrocarbons, Oils and Lipids: Diversity, Origin, Chemistry and Fate: Berlin, Germany, Springer, 746–767.

Taylor, S.R., and McLennan, S.M., 1985, The Continental Crust: Its composition and evolution. Blackwell, Malden, Mass.

Teichert, B.M.A., Eisenhauer, A., Bohrmann, G., Haase-Schramm, A., Bock, B., and Linke, P., 2003, U/Th systematics and ages of authigenic carbonates from Hydrate Ridge, Cascadia Margin: Recorders of fluid flow variations: Geochimica et Cosmochimica Acta, v. 67, p. 3845–3857, https://doi.org/10.1016/S0016-7037(03)00128-5.

Tian, J., Zhao, Q., Wang, P., Li, Q., and Cheng, X., 2008, Astronomically modulated Neogene sediment records from the South China Sea: Paleoceanography, v. 23, PA3210, https://doi.org/10.1029/2007PA001552.

Tong, H.P., Feng, D., Cheng, H., Yang, S.X., Wang, H.B., Min, A.G., Edwards, R.L., Chen, Z., and Chen, D.F., 2013, Authigenic carbonates from seeps on the northern continental slope of the South China Sea: New insights into fluid sources and geochronology: Marine and Petroleum Geology, v. 43, p. 260−271, https://doi.org/10.1016/j.marpetgeo.2013.01.011.

Wallmann, K., Riedel, M., Hong, W.L., Patton, H., Hubbard, A., Pape, T., Hsu, C.W., Schmidt, C., Johnson, J.E., Torres, M.E., Andreassen, K., Berndt, C., and Bohrmann, G., 2018, Gas hydrate dissociation off Svalbard induced by isostatic rebound rather than global warming: Nature Communications, v. 9, 83, https://doi.org/10.1038/s41467-017-02550-9.

Wang, M., Chen, T., Feng, D., Zhang, X., Li, T., Robinson, L.F., Liang, Q., Bialik, O.M., Liu, Y., and Makovsky, Y., 2022, Uranium-thorium isotope systematics of cold-seep carbonate and their constraints on geological methane leakage activities: Geochimica et Cosmochimica Acta, v. 320, p. 105−121, https://doi.org/10.1016/j.gca.2021.12.016.

Weldeab, S., Schneider, R.R., Yu, J.M., and Kylander-Clark, A., 2022, Evidence for massive methane hydrate destabilization during the penultimate interglacial warming: Proceedings of the National Academy of Sciences of the United States of America, v. 119, e2201871119, https://doi.org/10.1073/pnas.2201871119.

Westbrook, G.K., Thatcher, K.E., Rohling, E.J., Piotrowski, A.M., Pälike, H., Osborne, A.H., Nisbet, E.G., Minshull, T.A., Lanoiselle, M., James, R.H., Hühnerbach, V., Green, D., Fisher, R.E., Crocker, A.J., Chabert, A., Bolton, C., Beszczynska-Moller, A., Berndt, C., and Aquilina, A., 2009, Escape of methane gas from the seabed along the West Spitsbergen

continental margin: Geophysical Research Letters, v. 36, L15608, https://doi.org/10.1029/2009GL039191.

Wyrtki, K., 1961, Physical oceanography of the Southeast Asian waters. NAGA Report. La Jolla, Calif, v. 2, p. 1–195.

Zhang, G.X., Liang, J.Q., Lu, J.A., Yang, S.X., Zhang, M., Holland, M., Schultheiss, P., Su, X., Sha, Z.B., Xu, H.N., Gong, Y.H., Fu, S.Y., Wang, L.F., and Kuang, Z.G., 2015, Geological features, controlling factors and potential prospects of the gas hydrate occurrence in the east part of the Pearl River Mouth Basin, South China Sea: Marine and Petroleum Geology, v. 67, p. 356−367, http://dx.doi.org/10.1016/j.marpetgeo.2015.05.021.

Fig. 1. Location, age model of core GMGS2–16, and chronology of methane seepage from the South China Sea. (a) Locations of the GMGS2 drilling sites of the South China Sea. Pink dashed arrows and green arrows indicate the current directions of the South China Sea intermediate water and the North Pacific deep water, respectively (Lüdmann et al., 2005). Multi-beam topographic map of the Dongsha area is from Zhang et al. (2015). The map was generated with Ocean Data View. (b) The lithology of the studied cores and seep carbonates used for U/Th dating. Carbonate layer thickness is exaggerated to enhance visibility.

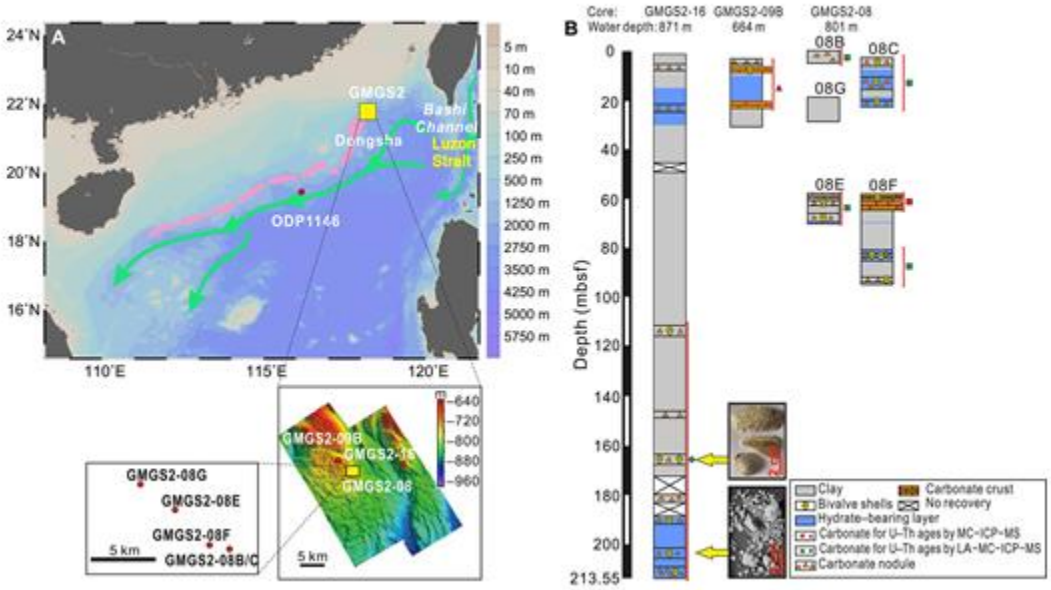

Fig. 2. Stable isotope compositions of seep carbonates from the Dongsha area (GMGS2–16, GMGS2–09B, GMGS2–08F, GMGS2–08E, GMGS2–08C, GMGS2–08B) of the South China Sea. Data of core GMGS2–09B is from Deng et al. (2019), data of core GMGS2–08F is from Chen et al. (2019), and data of core GMGS2–08B, GMGS2–08C, GMGS2–08E, and GMGS2–08F is from Chen et al. (2016a). The dashed lines indicate the $\delta^{18}O$ values of aragonite and calcite precipitating in equilibrium with seawater at corresponding present bottom water temperatures, respectively (Kim and O'Neil, 1997; Kim et al., 2007). The bottom water temperature is approximately 5.4 ºC for the Dongsha area, and the $\delta^{18}O$ of seawater is –0.3% V-SMOW (Feng and Chen, 2015). Considering differing $\delta^{18}O$ values such as 0.8‰ (VSMOW), i.e. to take into account potential $\delta^{18}O$ variability due to sea level change, calculated $\delta^{18}O$ compositions of aragonite precipitating in equilibrium with present-day SCS bottom water would be about 3.5‰ for the Dongsha area, hence being significantly lower than the $\delta^{18}O$ values measured in studied seep carbonates.

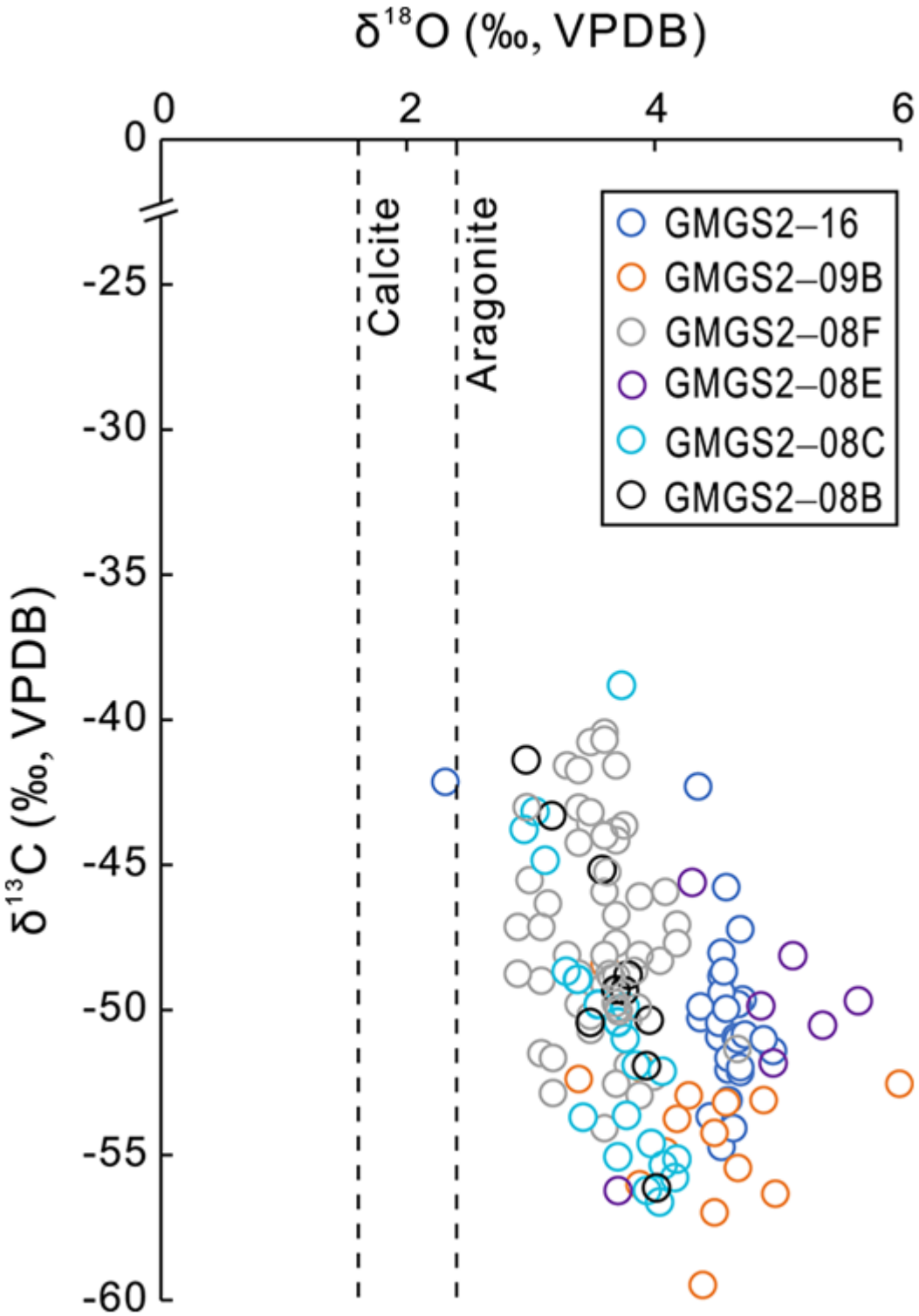
δ18O (‰, VPDB)
0
2
4
6
0
-25
-30
-35
-40
-45
-50
-55
-60
δ13C (‰, VPDB)
Calcite
Aragonite
GMGS2–16
GMGS2–09B
GMGS2–08F
GMGS2–08E
GMGS2–08C
GMGS2–08B

Fig. 3. Carbon and oxygen stable isotope compositions of planktonic (*Globigerinoides ruber*) (a, b), benthic (*Uvigerina peregrina*) foraminifera (c, d), stable carbon isotope of seep carbonates (e), and enrichment factor of Mo (Mo_{EF}) according to $Mo_{EF}=(Mo_{sample}/Al_{sample})/(Mo_{PAAS}/Al_{PAAS})$ with PAAS values from Taylor and McLennan (1985) (f) as well as content of $CaCO_3$ (g) in sediments of core GMGS2–16 from the Dongsha area of the South China Sea. The shaded areas indicate horizons affected by methane seepage, with $\delta^{13}C$ values of planktonic and benthic foraminifera possibly modified by encrusted authigenic carbonates. The red line is the five-point moving average of the oxygen isotope composition of planktonic foraminifera.

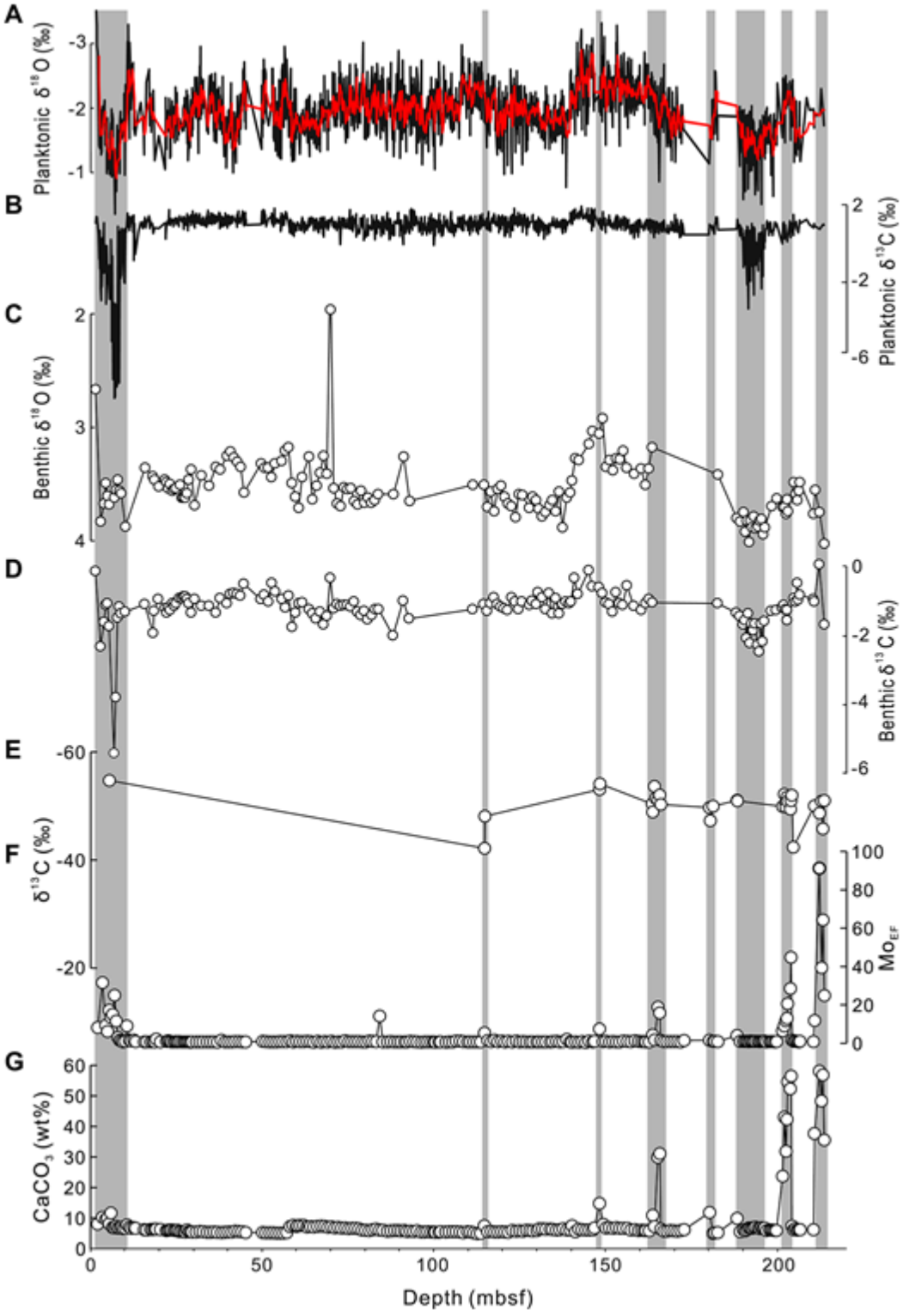
A
Planktonic δ18O (‰)
-3
-2
-1
B
2
-2
-6
Planktonic δ13C (‰)
C
Benthic δ18O (‰)
2
3
4
D
0
-2
-4
-6
Benthic δ13C (‰)
E
-60
F
δ13C (‰)
-40
-20
100
80
60
40
20
0
MoEF
G
CaCO3 (wt%)
60
50
40
30
20
10
0
0
50
100
150
200
Depth (mbsf)

Fig. 4. Age depth model for core GMGS2–16 based on (a) two ^{14}C dates (red squares), five sediment biostratigraphic ages (blue triangles; Chen et al., 2016b), the $\delta^{18}O$ planktonic foraminifera curve of GMGS2–16 correlated with (b) the $\delta^{18}O$ planktonic foraminifera curve ODP1146 (Clemens et al., 2008) and (c) the $\delta^{18}O$ benthic foraminifera curve ODP1146 (Clemens et al., 2008) and LR04 stack (Lisiecki and Raymo, 2005), and (d) the relative sea level from ODP1143 (Bates et al., 2014) and (e) sediment Mn/Fe and (f) Zr/Rb ratios of core GMGS2–16. Green and red crosses represent tie points. The shaded areas indicate horizons affected by methane seepage (see Fig. 3). B *E. huxleyi* Acme – First occurrence of Acme *Emiliania huxleyi*; T *G. ruber* (pink) – Last occurrence of *Globigerinoides ruber* (pink); B *E. huxleyi* – First occurrence of *Emiliania huxleyi*; B *G. ruber* (pink) – First occurrence of *Globigerinoides ruber* (pink); T *P. lacunosa* – Last occurrence of *Pseudoemiliania lacunosa* (all indicated by blue arrows).

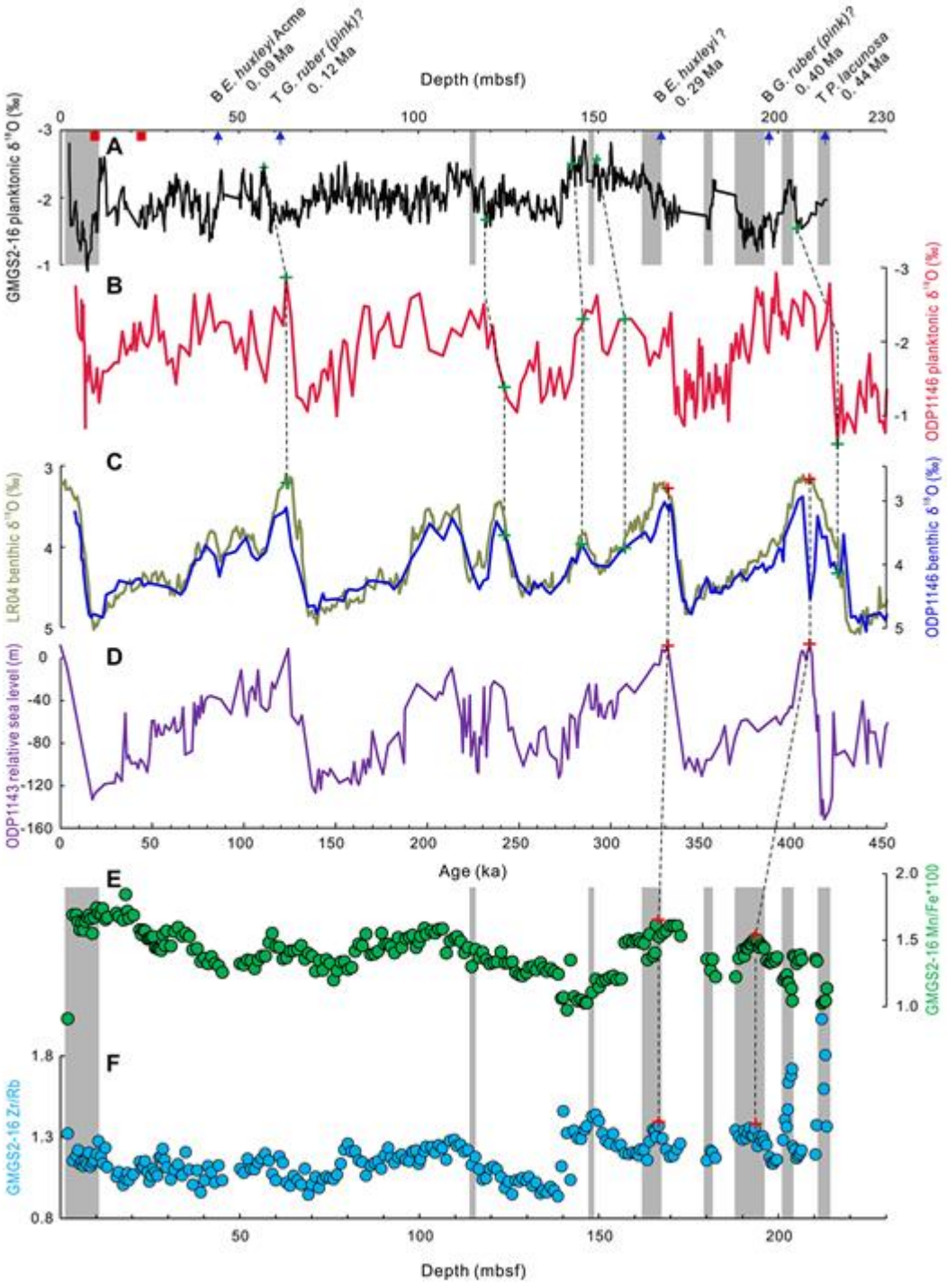
B E. huxleyi Acme
0. 09 Ma
T G. ruber (pink)?
0. 12 Ma
B E. huxleyi ?
0. 29 Ma
B G. ruber (pink)?
0. 40 Ma
T P. lacunosa
0. 44 Ma
Depth (mbsf)
GMGS2-16 planktonic δ18O (‰)
A
B
ODP1146 planktonic δ18O (‰)
C
LR04 benthic δ18O (‰)
ODP1146 benthic δ18O (‰)
D
ODP1143 relative sea level (m)
Age (ka)
E
GMGS2-16 Mn/Fe*100
F
GMGS2-16 Zr/Rb
Depth (mbsf)

Fig. 5. Age vs. depth of core GMGS2–16 from the Dongsha area of the South China Sea. ^{14}C dates (red squares), sediment biostratigraphic ages (blue triangles), tie points of sediment Mn/Fe and Zr/Rb ratios (red crosses), and tie points of $\delta^{18}O$ curve (green crosses).

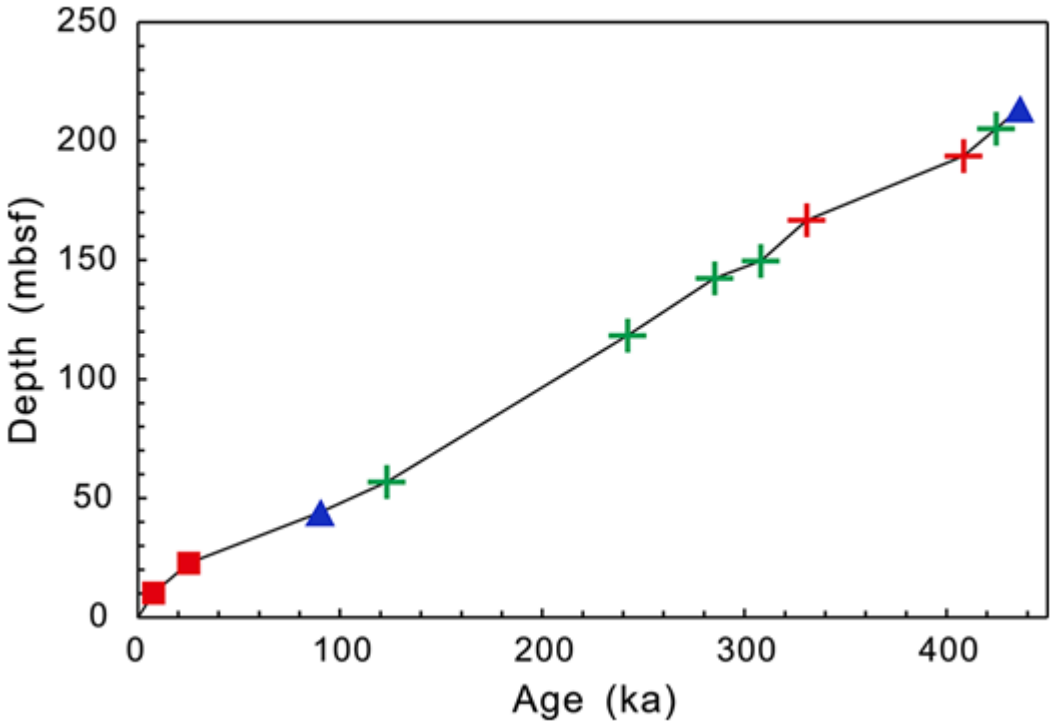

Fig. 6. Element and isotope composition of sediments in core GMGS2–16 from the Dongsha area of the South China Sea. (a) Mo content (μg/g), (b) enrichment of Mo (Mo_{EF}) according to Mo_{EF}= (Mo_{sample}/Al_{sample})/(Mo_{PAAS}/Al_{PAAS}) with PAAS values from Taylor and McLennan (1985), (c, d) carbon and oxygen isotope ratios (VPDB ‰) of seep carbonates, (e) total sulfur (TS) contents (wt%), (f) total organic carbon (TOC) contents (wt%), and (g) carbonate ($CaCO_3$) contents (wt%). The red dashed line indicates Mo_{EF} equal to 5. The shaded areas indicate the horizons of seep carbonates with Mo enrichment in sediment.

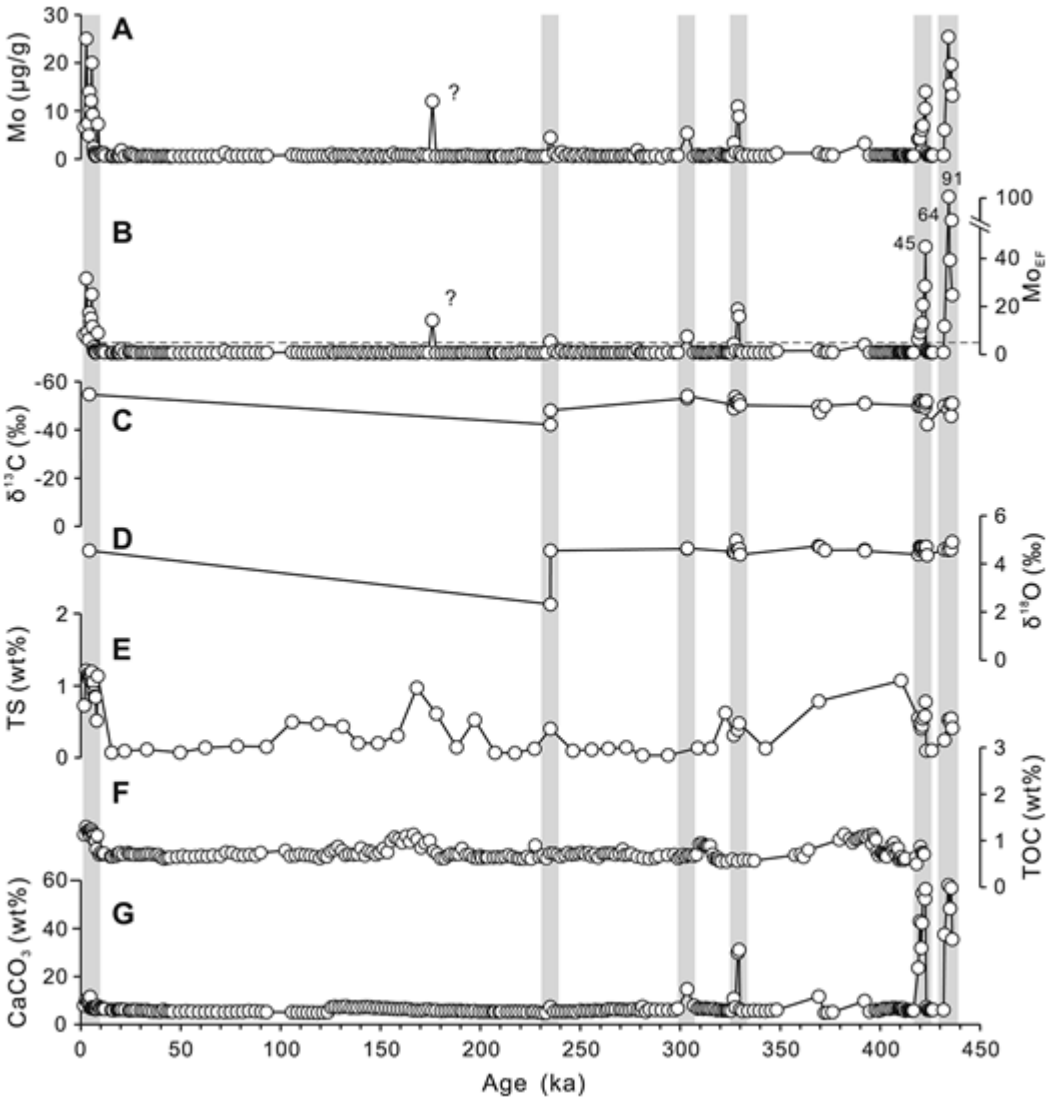

Fig. 7. Timing of seepage compared with bottom water temperature and sea level for the South China Sea during the past 450,000 years. (a) U-Th (error bars are 2s) ages of carbonates and ^{14}C ages of shells cemented by seep carbonate from the Dongsha areas (Feng and Chen, 2015; Chen et al., 2019; Deng et al., 2021). (b) Estimated bottom water temperature records from ODP1123 (South Pacific) based on Mg/Ca ratios of benthic foraminifera (Elderfield et al., 2012), ODP1143 (Southern South China Sea) derived from $\delta^{18}O$ values of benthic foraminifera (Bates et al., 2014), and Mg/Ca ratios of benthic foraminifera of core GH08–2004 (subtropical northwestern Pacific; Kubota et al., 2015). (c) Sea-level record from ODP1143 (Southern South China Sea; Bates et al., 2014). (d) $\delta^{18}O$ benthic foraminifera curve of ODP1146 (Clemens et al., 2008) and ODP1148 (Tian et al., 2008). (e) Benthic foraminifera $\delta^{18}O$ curve of the LR04 stack (Lisiecki and Raymo, 2005). Light green bars indicate peak interglacials.

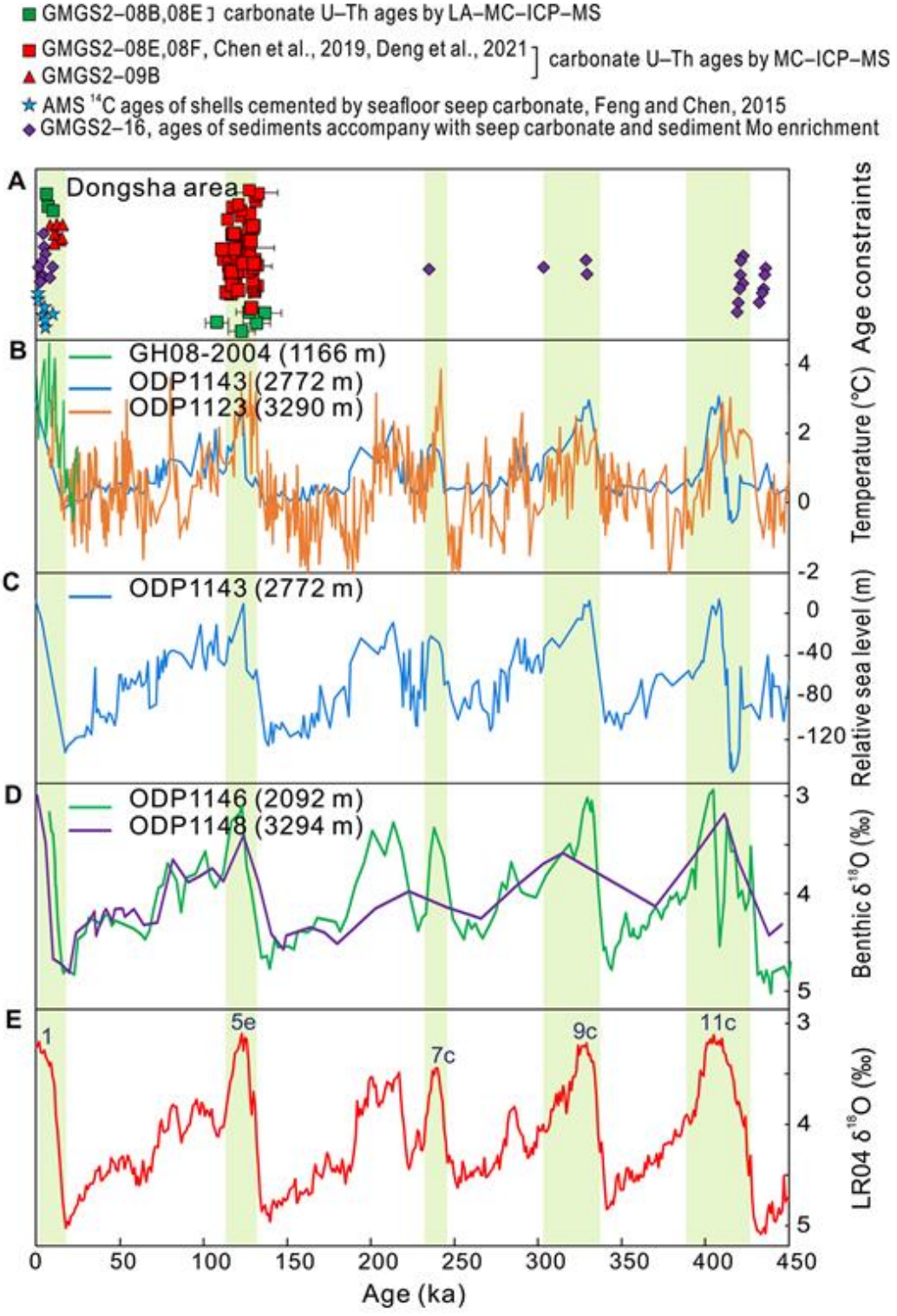
GMGS2–08B,08E carbonate U–Th ages by LA–MC–ICP–MS
GMGS2–08E,08F, Chen et al., 2019, Deng et al., 2021
GMGS2–09B
carbonate U–Th ages by MC–ICP–MS
AMS 14C ages of shells cemented by seafloor seep carbonate, Feng and Chen, 2015
GMGS2–16, ages of sediments accompany with seep carbonate and sediment Mo enrichment
A
Dongsha area
Age constraints
B
GH08-2004 (1166 m)
ODP1143 (2772 m)
ODP1123 (3290 m)
Temperature (°C)
C
ODP1143 (2772 m)
Relative sea level (m)
D
ODP1146 (2092 m)
ODP1148 (3294 m)
Benthic δ18O (‰)
E
1
5e
7c
9c
11c
LR04 δ18O (‰)
Age (ka)

Fig. 8. Changes of the base of methane hydrate stability zone (BHSZ) for the Dongsha area (GMGS2–16, water depth of 871 m) of the South China Sea during (a) the last glacial maximum (LGM) and (b) 105 to 140 ka. Red dots indicate the time of methane seepage (see Fig.7a).